RSC Advances

PAPER

View Article Online
View Journal | View Issue

Cite this: *RSC Adv.*, 2024, **14**, 21453

Modulating acid sites in Y zeolite for valorisation of furfural to get γ-valerolactone†

Malu Thayil Jayakumari and Cheralathan Kanakkampalayam Krishnan *

Furfural is a biomass-derived platform molecule that can be converted into a variety of useful products. Catalysts having appropriate balance between Lewis and Brønsted acid sites are suitable for valorisation of furfural. Lewis acidic metal ion incorporated zeolites were studied for this purpose. However, incorporating Lewis acidic metal ions into an alumino-silicate framework of a zeolite is a cumbersome process. Hence, an attempt has been made in this work to modulate the acid sites of Y zeolite *via* thermal treatment to effect controlled dealumination and use it for valorisation of furfural using isopropyl alcohol, which is a cascade transformation. The thermal treatment of zeolites changed the distribution of acid sites and increased the weak plus moderate to strong acid site ratio. Among the thermally dealuminated Y, beta and mordenite zeolites, with SiO_2/Al_2O_3 ratio 5.2, 25 and 20, only Y zeolite could yield γ-valerolactone, the final product of the aimed cascade transformation. Complete conversion of furfural and 52% γ-valerolactone yield could be achieved under the optimized conditions using NH_4Y zeolite thermally dealuminated at 700 °C (TY700). The better catalytic activity of TY700 could be correlated to a combination different factors such as framework structure, suitable weak plus moderate to strong acid site ratio, presence of both penta-coordinated and octahedral Al sites and balance between Brønsted and Lewis acid sites.

Received 26th April 2024
Accepted 1st July 2024

DOI: 10.1039/d4ra03113j

rsc.li/rsc-advances

1. Introduction

Biomass-derived sustainable fuels and chemicals are desired to decrease the dependence on non-renewable fossil resources. Lignocellulosic biomass is a type of plant-based material made up of lignin, cellulose, and hemicellulose, typically derived from trees, grasses and agricultural wastes. It is an attractive renewable source for producing a wide range of molecules having potential uses to produce industrial chemicals, solvents and fuels.[1] Different processes have been employed for breaking down the complex lignocellulosic biomass to get useful products and molecules.[2–4] Lignocellulosic biomass upon hydrolysis can yield furanic molecules which can be further employed as precursors for production of a wide range of important chemicals including solvents, monomers, fuels, and fuel additives.[5] Furfural (FFR) is one of the thirty platform molecules obtained *via* hydrolysis of lignocellulosic biomass[6–8] and it is mass-produced from hemi cellulosic feedstocks.[9,10] Furfural is highly reactive due to the presence of an aldehyde functional group and hence it can be easily functionalized *via* different chemical routes to get molecules of higher value.[11] The different value-added molecules, obtained from FFR are furfuryl alcohol (FA), furfuryl alkyl ethers (FE), levulinic acid (LA), alkyl levulinates (AL), α & β-angelica lactones (AGL) and γ-valerolactone (GVL).[10,12–15]

Conventionally, catalytic reduction of FFR using molecular hydrogen and a noble metal catalyst was used to obtain the value-added molecules. Controlling the reaction pathways and the degree of hydrogenation using a selective catalyst is always a challenge in catalytic hydrogenation of furfural.[16] Catalytic transfer hydrogenation (CTH) or Meerwein–Ponndorf–Verley (MPV) reduction of FFR using alcohols as hydrogen sources is considered as an alternative to the conventional catalytic hydrogenation. CTH of FFR is normally carried out using secondary alcohols such as isopropanol (IPA) and secondary butanol as hydrogen donors in the presence of a Lewis acid-base catalyst.[17,18] Based on the reaction parameters,[19] nature of the catalyst,[10] and the kind of solvent used,[20] valorisation of FFR may proceed in different pathways. For example, FFR valorisation using isopropanol in the presence of acid catalysts may proceed through different steps and produce a series of products as shown in Scheme 1.[12,21–23] If Lewis acid sites suitable for MPV reduction are present, the main pathway followed is CTH of FFR into furfuryl alcohol and its subsequent etherification to form furfuryl ether. If Brønsted acid sites are present along, FFR can undergo acetalization with the alcohol and form diisopropyl furfuryl acetal. Then, by elimination of an alcohol in the presence of acid sites, it can form isopropyl furfuryl ether. In the next step, furanic ring opening of the furfuryl ether gives rise to

Department of Chemistry, School of Advanced Sciences, Vellore Institute of Technology, Vellore 632014, India. E-mail: Cheralathan.k@vit.ac.in

† Electronic supplementary information (ESI) available: X-ray diffraction pattern, N_2 adsorption isotherms, TPD of NH_3 profiles and ^{27}Al MAS NMR, pyridine adsorption-FTIR and GC-MS spectra. See DOI: https://doi.org/10.1039/d4ra03113j

isopropyl levulinate. Finally, the CTH of isopropyl levulinate and further lactonization may yield GVL (Scheme 1). Lewis acid sites present in zirconium, tin, and titanium containing catalysts including zeolites are known to catalyse MPV reduction.[24–28] However, the presence of both Lewis and Brønsted acid sites within the catalyst is important for promoting conversion of the different intermediates shown in Scheme 1 and finally to form GVL. For instance, when Sn- and Zr- loaded beta zeolite is an effective catalyst for the MPV reduction of FFR to furfuryl alcohol,[29] Zr supported on dealuminated zeolite Y[30] and bimetallic Sn–Zr supported on dealuminated Y zeolite have been shown to yield GVL.[31] The importance of Lewis and Brønsted acid sites in converting FFR to GVL has been demonstrated by Bui *et al.* using a mixture of Zr-beta and Al-MFI zeolite as catalyst.[32]

The introduction of Lewis acidic metal into the zeolite framework is usually carried out either *via* direct synthesis[33,34] or *via* post synthetic modifications;[35,36] the latter includes dealumination/removal of Al from zeolite and subsequent metal ion incorporation involving cumbersome multiple step procedure.[37] In this regard, generating Lewis acid sites stemming from Al intrinsic to zeolites and exploiting the associated Brønsted acid sites of the same zeolite to catalyse FFR valorisation would avoid the use of costly metals and tedious multistep synthesis procedures. For instance, as reported recently, properly tuning the coordination environment of Al in Y zeolite *via* controlled thermal dealumination can produce a catalyst suitable for MPV reduction of levulinic acid and isopropyl levulinate to yield GVL.[38] During dealumination procedure, when zeolite is treated at temperatures >500 °C, in the presence of air (thermal treatment) or air saturated with water vapor (steam treatment), Si–(OH)–Al bonds in the tetrahedral framework are broken completely or partially leading to either extra-framework aluminium (EFAl) or partially detached Al sites.[38] Through this dealumination process, different Al sites such as framework-associated, partially detached, distorted-tetrahedral or penta-coordinated Al, and hexa-coordinated extra-framework aluminium could be formed.[39] The presence of these multiple Al species detached from the zeolite framework can create Lewis acid sites of different characteristics, and further, along with these Lewis acid sites, Brønsted acid sites originated from tetrahedral Al will coexist within the same zeolite,[39] making the dealuminated zeolite suitable for cascade reactions. With this background, in this work, we aim at creating a suitable catalyst *via* controlled dealumination of zeolite framework for conversion of FFR to GVL. This method has advantage as acid sites could be modulated in a relatively simple procedure without the need of incorporating an external Lewis acidic metal onto the zeolite framework. To fulfil this, ammonium forms of Y, beta and mordenite zeolites were thermally treated at different conditions to effect dealumination. After proper physicochemical characterization, the catalytic performance of the dealuminated zeolites were compared. The nature & distribution of acid sites and different Al species generated during the thermal and steam treatment were correlated with FFR conversion and GVL formation.

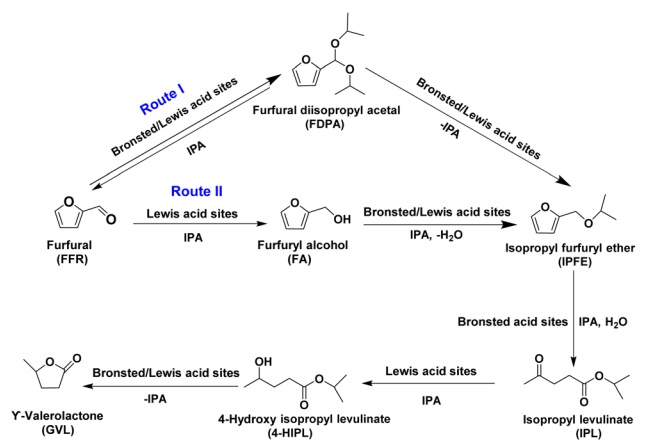

Scheme 1 Cascade reaction pathway of furfural to γ-valerolactone transformation.

2. Experimental

2.1 Materials

Ammonium forms of Y zeolite (NH_4Y) (CBV500, SiO_2/Al_2O_3 = 5.2), beta zeolite (CP81E, SiO_2/Al_2O_3 = 25), and mordenite (CBV21A, SiO_2/Al_2O_3 = 20) were obtained from Zeolyst International, USA. Furfural (98%) and levulinic acid (98%) were obtained from Sigma-Aldrich, India. Isopropanol (99%) was procured from SD Fine chemicals, India. Furfuryl alcohol (>98%), γ-valerolactone (>98.0%), α-angelica lactone (>98.0%), mesitylene (>98.0%), were purchased from Tokyo Chemical Industry (India) Private Ltd. Isopropyl levulinate (IPL) was synthesized in the laboratory and confirmed by spectroscopic methods.[38]

2.2 Catalyst preparation

The thermally treated zeolite catalysts were prepared as reported earlier.[38] Briefly, NH_4Y zeolite was heated in the presence of air (thermal treatment) or air saturated with water (steam treatment) at different temperatures ranging from 500–800 °C. The catalysts thus obtained were coded as TYX for thermal treated samples and SYX for steam treated samples, where X denotes the treatment temperatures. In this manner, different catalysts named as TY500, TY600, TY700, TY800, SY500 and SY700 were prepared. NH_4 forms of beta and mordenite zeolites were also thermally treated at 500, 700 and 800 °C and named as TB500, TM500, TB700, TM700, TB800 and TM800. In these catalyst codes, Y, B and M denotes Y, beta and mordenite respectively.

2.3 Catalysts characterization

Bruker D8 Advance X-ray diffractometer was used to collect the X-ray diffraction (XRD) patterns of the prepared catalysts. Cu Kα X-ray (λ = 1.5406 Å) was used and the catalyst powders were scanned starting from 5 to 90° 2θ. Multipoint Brunauer–Emmett–Teller (BET) surface area of the catalysts was determined using nitrogen adsorption at 77 K using Quantachrome, ASiQwin Autosorb iQ Station. The catalysts were heated at 150 °

C for 24 h during outgassing step carried out before N_2 adsorption. *t*-Plot method was used to determine micropore surface area and micropore volume. Microtrac, BELCAT II catalyst analyzer equipped with thermal conductivity detector (TCD) was used to study temperature programmed desorption of ammonia (TPD-NH_3). The catalyst was heated and outgassed at 250 °C for 2 h. After the outgassing step, the catalyst was cooled down to 100 °C and ammonia gas (20% in helium) was allowed to flow (flow rate = 15 mL min^{-1}) for 30 min. Then, the catalyst was purged with He for 30 min. After purging, the catalyst was heated from 100 to 700 °C (heating rate = 10 °C min^{-1}) under He flow to facilitate desorption of ammonia. Jeol ECX400 multinuclear FT-NMR spectrometer was used to obtain ^{27}Al MAS NMR spectra of the catalysts. $AlCl_3$ was used as the reference. The catalyst samples were spun at the speed of 10 kHz at radio frequency of 104 MHz. Jasco FT-IR 4100 spectrometer equipped with MCT detector was utilized to obtain pyridine FT-IR spectra of the catalysts. About 40 mg of catalyst was pressed into the form of a disc and then heated at 200 °C for 3 h under vacuum in an IR cell to remove adsorbed water. After this step, pyridine vapour was allowed to adsorb on the catalyst at room temperature. The excess pyridine was removed by applying vacuum and then the spectra were recorded.

2.4 Catalytic reaction

The reaction was performed in a 100 mL high-pressure reactor made of stainless-steel and having Teflon lining inside. In a typical experiment, the reactor was charged with 1 mmol FFR dissolved in 20 mL of isopropanol (IPA) followed by addition of predetermined quantity of catalyst and mesitylene as internal standard. The reaction mixture was magnetically stirred at 1000 rpm using a magnetic pellet and heated to different temperatures between 100 to 190 °C. The reaction was carried out for different time durations between 1 to 12 h. After the reaction, the reactor was cooled down to room temperature and the reaction mixture was centrifuged to remove the catalyst and analyzed by using a gas chromatograph (Shimadzu GC 2010 gas chromatograph (GC)), Stabilwax-DA capillary column (30 m, 0.25 mm ID, 0.25 μm) equipped with flame ionization detector. The standards of the expected products (furfuryl alcohol, isopropyl levulinate, α-angelica lactone, levulinic acid and GVL) were used for identification of the products in GC based on their retention time. The products were also confirmed using Gas Chromatography/Mass Spectrometry (GC/MS) (Model: PerkinElmer Clarus 680/PerkinElmer Clarus 600) equipped with Elite-5ms capillary column (30 m × 0.25 mm I.D. × 0.25 μm). The concentrations of the individual products in the reaction mixture were determined by using GC standard calibration plots. As the standards are not available, the quantification of furfural diisopropyl acetal (FDPA) and isopropyl furfuryl ether (IPFE) was done using the calibration plots of FA and IPL respectively. The presence of FDPA and IPFE was also confirmed by the GC-MS analysis (See ESI, Fig. S1 and S2†). The reaction conditions for TOF_{FFR} analysis were optimized to get below 50% conversion of furfural. The TOF_{FFR} of the catalysts were calculated based on FFR conversion and acid sites measured from TPD-NH_3 profiles. The following equations were used to find conversion of furfural, product yield, product selectivity and turnover frequency (TOF_{FFR}):

$$\text{Conversion}(\%) = \frac{\text{Moles of furfural taken} - \text{moles of furfural unreacted} \times 100}{\text{Moles of furfural taken}}$$

$$\text{Yield}(\%) = \frac{\text{Product obtained(in moles)} \times 100}{\text{Furfural taken(in moles)}}$$

$$\text{Selectivity}(\%) = \frac{\text{Product obtained(in moles)} \times 100}{\text{Furfural converted(in moles)}}$$

$$TOF_{FFR} = \frac{\text{Number of moles of furfural converted in to products}}{\text{Number of moles of acid sites in catalyst} \times \text{reaction time(h)}}$$

3. Result and discussion

3.1 X-ray diffraction and N_2 adsorption analysis

Powder X-ray diffraction analysis was carried out to determine crystallinity and structure of the prepared zeolite catalysts and the diffraction patterns are shown in ESI Fig. S3.† In Y zeolites, the peak intensity showed a decreasing trend moving from TY500 to TY800 and SY500 to SY700. In beta zeolites, TB500 & TB700 the XRD patterns were of similar shape and intensities, but in TB800 the peak intensity decreased. In mordenite, the peak intensity decreased moving from TM500 to TM800. The decrease in intensity of the peaks in X-ray diffraction patterns of zeolites, while increasing the treatment temperature greater than 500 °C could be due to breaking and disappearance of Si–(OH)–Al bridges leading to detachment of aluminium from the framework and the resulted structural damage. Nitrogen adsorption isotherms, multipoint BET surface area and pore volume data of the catalysts are given in Fig. S4† and Table 1. As a general trend, increasing thermal and steam-treatment temperature decreases multipoint BET surface area, and micropore surface area of the catalysts. The decrease in X-ray diffraction peak intensity, multipoint point BET surface area and micropore surface area is likely due to structural damage caused to the framework of the zeolites upon heating at higher temperatures.[38]

3.2 Characterization of acid sites

The nature of acid sites existing in the prepared catalysts were investigated by temperature programmed desorption of NH_3. The desorption profiles were deconvoluted using Gaussian function to understand the distribution of weak, moderate, and strong acid site and presented in Fig. S5 in ESI.† In the TPD profiles, the desorption of NH_3 between 100 to 250 °C was ascribed to weak acid sites; the desorption from 400 to 600 °C

Table 1 Surface area and pore volume of the prepared catalysts

Catalyst	BET surface area ($m^2\ g^{-1}$)	Micropore surface area ($m^2\ g^{-1}$)	External surface area ($m^2\ g^{-1}$)	Micropore volume (V_{micro}) ($cm^3\ g^{-1}$)	Total pore volume (V_{total}) ($cm^3\ g^{-1}$)	$V_{(micro)}/V_{(total)}$ ($cm^3\ g^{-1}$)
TY500	746	699	47	0.259	0.379	0.683
TY600	717	671	46	0.256	0.371	0.690
TY700	713	657	56	0.250	0.369	0.677
TY800	675	618	57	0.237	0.380	0.623
SY500	726	667	59	0.255	0.371	0.687
SY700	664	611	53	0.234	0.372	0.629
TB500	500	352	148	0.142	0.809	0.175
TB700	466	314	152	0.127	0.714	0.177
TB800	413	249	164	0.107	0.632	0.169
TM500	387	305	82	0.120	0.285	0.421
TM700	290	163	127	0.066	0.204	0.323
TM800	224	53	171	0.042	0.189	0.222

Table 2 Comparison of number of acid sites obtained from temperature programmed desorption of NH_3

Catalyst	Weak ($mmol\ g^{-1}$)	Moderate ($mmol\ g^{-1}$)	Strong ($mmol\ g^{-1}$)	Total ($mmol\ g^{-1}$)
TY500	0.69	0.44	0.33	1.46
TY600	0.70	0.42	0.22	1.34
TY700	0.70	0.40	0.15	1.25
TY800	0.70	0.39	0.09	1.18
SY500	0.69	0.35	0.26	1.312
SY700	0.59	0.35	0.13	1.087
TB500	0.68	0.33	0.19	1.20
TB700	0.53	0.25	0.11	0.896
TM500	0.68	0.23	0.39	1.30
TM700	0.47	0.17	0.20	0.842

was related to strong acid sites; the desorption feature from 250 to 400 °C was correlated to moderate acid sites.[38,40a–c,41a,b] All the zeolites studied showed three desorption features corresponding to weak, moderate, and strong acid sites. A comparison of total number of acid sites and contribution from weak, moderate, and strong acid sites is presented in Table 2. Upon thermal treatment of NH_4Y zeolite from 500 to 800 °C, a gradual decrease in total number of acid sites could be observed.

Further, it can be noticed that the strong acid sites of the Y zeolite are affected the most while increasing thermal treatment temperature. The moderate acid sites of Y zeolite are affected to a lesser extent, while weak acid sites are retained during the thermal treatment. The decrease in the amount of strong acid sites in Y zeolite with increasing temperature can be attributed to breaking and disappearance of Si–(OH)–Al bridges that are responsible for the strong Brønsted acid sites. When this occurs, the resulted detachment of aluminium from the framework may lead to different Al species (Section 3.3). Compared to TY500 and TY700, their steam treated counterparts, SY500 and SY700 showed lower total number of acid sites (TY500 = 1.46 mmol g^{-1}, SY500 = 1.312 mmol g^{-1}, TY700 = 1.25 mmol g^{-1}, SY700 = 1.087 mmol g^{-1}). Further it can be noticed that steam treatment affected all the three, weak, moderate, and strong acid sites without any selectivity. In the case of beta and mordenite zeolites, compared to thermal treatment at 500 °C, thermal treatment at 700 °C drastically decreased the total number of acid sites, and all the three types of acid sites were affected.

The chart of percentage distribution of weak, moderate & strong acid sites in the catalysts is given in Fig. S6 in ESI.† The chart indicates that when the treatment temperature is increased, percentage of strong acid sites in Y zeolites decreases and at the same time percentage of weak acid sites increases. It can be also noted that the distribution of moderate acid sites in Y zeolites is not affected much while varying the thermal treatment temperature. The similar trend was observed upon steam treatment in the case of SY500 & SY700 and thermal treatment in the cases of TB500 & TB700 and TM500 & TM700.

3.3 Coordination environment of aluminium

The ^{27}Al-MAS NMR spectroscopy was utilized to assess the nature of the coordination environment of aluminium in the studied catalysts. Based on the NMR chemical shift values, different aluminium sites, such as tetrahedral Al (Al^{IV}-I, Al^{IV}-II) (chemical shift range = 55–65 ppm), penta-coordinated Al (Al^{V}) (chemical shift range = 30–40 ppm) and octahedral Al (Al^{VI}) (chemical shift range = 0–6 ppm), also known as extra-framework Al could be identified.[42,43] Further, based on the area under the resonance peaks in the deconvoluted ^{27}Al-MAS NMR spectra (see ESI Fig. S7†), the distribution of the different aluminium sites was calculated and presented in Fig. S8 in ESI.†

In NH_4Y zeolite before thermal treatment, Al^{IV}-I, Al^{V} & Al^{VI} sites are present. While increasing the thermal treatment temperature of NH_4Y from 500 to 700 °C (TY500, TY600 and TY700), Al^{IV}-II starts to appear and at the same time, A^{V} & Al^{VI} sites tend to increase at the expense of Al^{IV}-I sites. However, this trend is broken in TY800, wherein, Al^{IV}-I and Al^{VI} sites are present, Al^{IV}-II sites are absent and Al^{V} sites decreased. In SY500, like TY500, Al^{IV}-I, Al^{IV}-II, A^{V} & Al^{VI} sites can be seen, but SY700 & TY700 show completely different distribution of the Al sites. In SY700, Al^{IV}-II sites are absent and only a smaller percentage of Al^{V} sites are present compared with TY700.

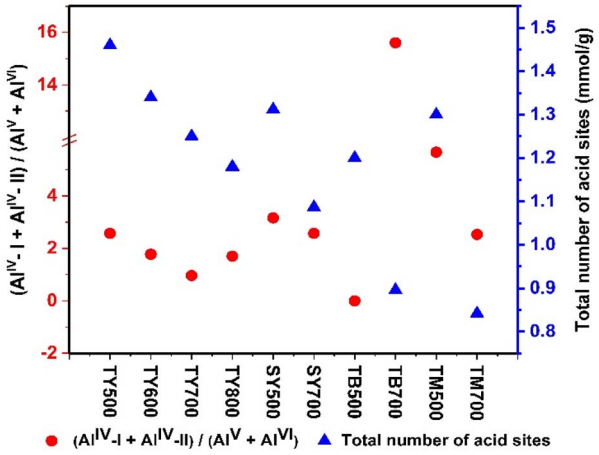

Fig. 1 Correlation between (Al^{IV}-I + Al^{IV}-II)/(Al^{V} + Al^{VI}) ratio and total number of acid sites.

In the case of beta zeolites, TB500 have only Al^{IV} sites, but while increasing the treatment temperature to 700 °C (TB700), Al^{VI} sites appeared. In TM500, Al^{IV}-I, Al^{IV}-II & Al^{VI} sites are observed. While increasing the thermal treatment temperature from 500 to 700 °C, in TM700, Al^{IV}-II & Al^{VI} sites tend to increase at the expense of Al^{IV}-I sites. It can be noted that in beta and mordenite zeolite samples, Al^{V} sites are totally absent. Importantly, compared with all the other zeolites prepared and studied here, in TY700, greater percentage of framework associated penta-coordinated, A^{V} species are present. Table S1 in ESI† compares (Al^{IV}-I + Al^{IV}-II)/(Al^{V} + Al^{VI}) ratio obtained for all the prepared catalysts and the lowest ratio is obtained for TY700, which indicates that it has more Al dislodged from the zeolite framework. Fig. 1 correlates (Al^{IV}-I + Al^{IV}-II)/(Al^{V} + Al^{VI}) ratio with total acid sites, which indicates that when dealumination of the framework occurs and Al^{V}, Al^{VI} sites are generated the total number of acid sites are decreased.

3.4 Catalytic activity studies

The prepared zeolites were studied as catalysts for converting FFR to value-added products in the presence of IPA under same reaction conditions and the results are compared in Table 3. On all the catalysts studied, isopropyl levulinate (IPL) was obtained as the major product. Furfural diisopropyl acetal, isopropyl furfuryl ether and γ-valerolactone were obtained as minor products. Some unidentified products in trace quantities (<1%) and acetone & diisopropyl ether, the products obtained from IPA were also observed in the reaction mixtures. A separate reaction run was also performed in the absence of catalyst under the same reaction conditions, and none of the mentioned products were detected, which confirms the role of catalyst in the reaction. No furfuryl alcohol was detected over any of the zeolites under the studied reaction conditions, but formation of furfural diisopropyl acetal was observed over all the catalysts.

Further, no furfuryl alcohol formation was observed on Y zeolites even at much lower conversion rates under different reaction conditions as discussed in the later part of this article. These results indicate that over the catalysts, the cascade reaction proceeds through acetalization of furfural (route I in Scheme 1). In fact, acetalization of furfural and reduction of furfural to form furfuryl alcohol are competitive reactions[44,45] and the former suppresses the later and requires acid sites.[45,46] Different zeolites possessing strong acid sites were found to efficiently catalyse acetalization of furfural.[47,48] Hence, it is likely that FFR to FDPA reaction outperformed FFR to FA conversion in this study because all the catalysts possess strong acid sites. As a general trend, increasing the thermal treatment temperature of the Y zeolites from 500 to 700 °C (TY500, TY600 & TY700), increased the conversion of FFR. Similarly, increasing the steam treatment temperature from 500 (SY500) to 700 °C (SY700) increased the conversion. However, compared with TY700, on SY700 and TY800, the conversion of FFR decreased probably due to large decrease in total surface area (SA of TY700 = 713 $m^2\ g^{-1}$, SA of SY700 = 664 $m^2\ g^{-1}$, SA of TY800 = 675 $m^2\ g^{-1}$). The difference in conversion observed among the different framework type zeolites Y, beta and mordenite could be due their structural difference and surface area. While Y and beta zeolites have three-dimensional pore network with the former having super cages, mordenite possesses two-dimensional pore system. Further, mordenite zeolites prepared in this study show relatively lower surface area compared to Y and beta zeolites. So, the relatively lower

Table 3 Catalytic activity of the different zeolites (*reaction conditions: FFR = 100 mg (1 mmol), IPA = 20 mL, catalyst = 100 mg, temp. = 175 °C, time = 6 h. (possible error in conversion & selectivity = ± 2%))

Entry	Catalyst	FFR conversion (%)	FDPA selectivity (%)	IPFE selectivity (%)	IPL selectivity (%)	GVL selectivity (%)
1	TY500	60	18	3	74	4
2	TY600	64	17	10	67	5
3	TY700	98	1	—	76	21
4	TY800	55	11	7	73	8
5	SY500	63	7	2	83	5
6	SY700	81	5	19	54	3
7	TB500	78	5	—	95	—
8	TB700	88		—	100	—
9	TB800	62	17	—	82	—
10	TM500	30	9	—	91	—
11	TM700	52	5	48	47	—
12	TM800	9	18	42	40	—

conversions obtained on TM500, TM700 and TM800 compared to their Y and beta counterparts could be due to these differences.

However, apart from pore structure and surface area, the nature of the acid sites and their distribution might also play a role in the catalytic activity. Since acetalization is found to be the starting point of the cascade reaction (Scheme 1), the acid sites required for the acetalization reaction could be the determining factor for conversion of furfural. Song *et al.* studied acetalization of furfural with 1,2 propanediol over SAPO-34, SAPO-11, USY, HY and HZSM-5 zeolites and found that SAPO-34 is found to be best performing catalyst due to greater number of moderate and strong acid sites.[47] However, when USY and HY zeolites were compared for the same acetalization reaction, USY (11) zeolite with more weak acid sites (2.12 mmol g^{-1}) and moderate plus strong acid sites (0.60 mmol g^{-1}) combination was found to be the better catalyst than HY (weak acid sites = 1.92 mmol g^{-1}, moderate plus strong acid sites = 0.58 mmol g^{-1}).[47] Another study reported that H-USY zeolite (Si/Al = 6, acid sites = 835 μmol g^{-1}) is better catalyst than Hβ (Si/Al = 12.5, acid sites = 855 μmol g^{-1}) and H-mordenite (Si/Al = 10, acid sites = 1656 μmol g^{-1}) for acetalization furfural with ethanol.[48] A comparative study on acetalization of furfural with ethanol found that weak acid sites and mesoporosity present in hierarchical beta zeolite makes it a better catalyst than conventional beta zeolite.[49] Apart from Brønsted acid sites, acetalization of furfural has been reported even on purely Lewis acidic catalysts.[29]

In the present study, the characterization of acid sites of Y zeolites discussed under Section 3.2 indicated that total number of acid sites decrease while increasing thermal and steam treatment temperature. Strong acid sites of the zeolites are affected the most during such treatments, whereas weak and moderate acid sites are not relatively affected much. So, in order to correlate the acid sites distribution and FFR conversion, a correlation graph between, FFR conversion and weak + moderate acid sites to strong acid sites ratio ((W + M)/S ratio) of the catalysts was plotted (Fig. 2(a)). From the graph, it could be seen that within the specific framework type zeolites (Y, beta & mordenite), there is a correlation between FFR conversion and (W + M)/S ratio; when the ratio increases, FFR conversion also increases. Overall, weakening the acid sites by dealumination improves the conversion of furfural, this is in line with previous reports.[47–49] However, in TY800, this trend is not followed probably due to its much higher, more than optimum (W + M)/S ratio. Further, to support these conclusions, as shown in Fig. 2(b), a linear relationship was obtained between TOF_{FFR} and (W + M)/S ratio of the thermally dealuminated zeolites. The highest TOF_{FFR} value, 3.6 h^{-1} obtained for TY700 indicated that it is the best among the catalyst studied. A similar graph of TOF_{FFR} *vs.* weak acid sites/(moderate acid sites + strong acid sites) ratio was plotted, but no linear relationship could be obtained (Fig. 2(c)). Though IPL was the major product formed over all the different framework zeolites studied, GVL was formed only on Y zeolites. In this aspect, TY700 was found to be the most suitable catalyst for GVL production as it showed 98 ± 2% conversion of FFR and 20 ± 0.4% yield of GVL (Table 3). Incidentally, TY700 is the catalyst having optimum (W + M)/S ratio and higher number of penta-coordinated (Al^{V}) and octahedral aluminium (Al^{VI}) sites (from Section 3.3, ^{27}Al MAS NMR spectroscopy studies). Among the different framework type zeolites studied here, zeolite Y has more Al (SiO_2/Al_2O_3 = 5.2) than beta (SiO_2/Al_2O_3 = 25) and mordenite (SiO_2/Al_2O_3 = 20), hence, probably, it is more susceptible for dealumination and formation penta-coordinated (Al^{V}) and octahedral aluminium (Al^{VI}) sites. In beta and mordenite zeolites though framework eliminated Al species could be generated, they found to be easily reinserted into the framework.[50–52] Actually, Lewis acid sites in zeolites can stem from Al^{III}, A^{V} and extra-framework Al^{VI} species.[39,53] However, the tri-coordinated Al sites (Al^{III}) are in an extremely distorted local environment and normally not visible in the ^{27}Al MAS NMR spectrum because of their strong quadrupolar interactions[54,55]

Previous study indicated that octahedral extra-framework Al (EFAL) species introduced onto Y and beta zeolites enhance reduction of 4-*tert*-butylcyclohexanone to its corresponding alcohol, as Lewis acidity of the catalysts is increased.[37,56] In another study, Lewis acid sites related to penta-coordinated Al (A^{V}) species in Y zeolite were found to be the potential Lewis acid sites suitable for reduction of levulinic acid and IPL to GVL.[38] However, in FFR to GVL conversion *via* MPV reduction, presence of both Brønsted and Lewis sites are important to get GVL.[27,32,57,58] Further, the ratio between Brønsted acid sites/Lewis acid sites (B/L) ratio should be properly tuned for

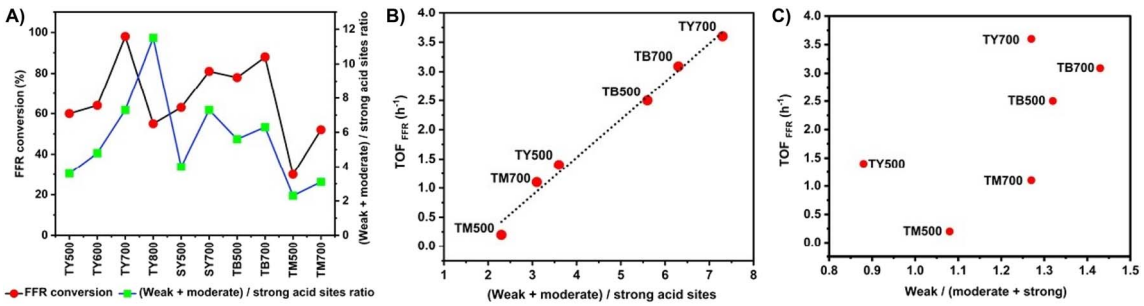

Fig. 2 (a) Furfural conversion *vs.* (weak + moderate)/strong acid sites ratio, (b) linear relationship between (weak + moderate)/strong acid sites ratio and TOF_{FFR}, (c) non-linear relationship between weak/(moderate + strong acid) sites ratio and TOF_{FFR}.

higher GVL yields and selectivity.[22,59] In this regard, the B/L ratio of 0.5 to 0.6 is found to be the optimum to maximize the yield/selectivity of GVL.[22,59] The pyridine-FTIR spectra of TY500 & TY700 are shown in Fig. S9 (see ESI).† The pyridine-FTIR spectra indicated the presence of both Brønsted and Lewis acid sites which are required for facilitating FFR to GVL transformation. The B/L ratio of the TY500 and TY700 were calculated based on the peak areas under the absorbance bands at 1545 cm^{-1} and 1450 cm^{-1} in the spectra. For TY700, the B/L ratio was found to be 0.63 and the same for TY500 was 0.71. The B/L ratio of TY700 (0.63) is close to the B/L ratio requirement reported previously for higher selectivity of GVL.[22,59] So, the better catalytic activity of TY700 compared to other catalysts studied here might be due to combination different factors such as framework structure, suitable (W + M)/S acid sites ratio, presence of both Al^{V} and Al^{VI} sites and proper balance between Brønsted and Lewis acid sites.

3.5 Influence of reaction parameters

As TY700 catalyst exhibited the best catalytic activity among the studied catalyst in terms of conversion of FFR and selectivity towards GVL, it was further explored to understand the influence of different reaction parameters. The reaction was carried out at different temperatures such as 100, 150, 175 and 190 °C and the influence of temperature on conversion of FFR and yields of the products are compared in Fig. 3. While increasing the reaction temperature from 100 to 175 °C, conversion increased from 24 ± 0.5% to 98 ± 2% and it became 100% at 190 °C. It could also be observed that at all the studied temperatures, IPL was the major product. No GVL was formed at 100 °C but it started to form (GVL yield = 8 ± 0.2%) when temperature was increased to 150 °C, and its yield reached to 20 ± 0.4% at 175 °C. A drop in GVL yield was observed when the reaction temperature was further increased to 190 °C. The decrease in GVL yield at 190 °C can be attributed to the formation of by-products as suggested by Rao *et al.*[60] At 100 °C

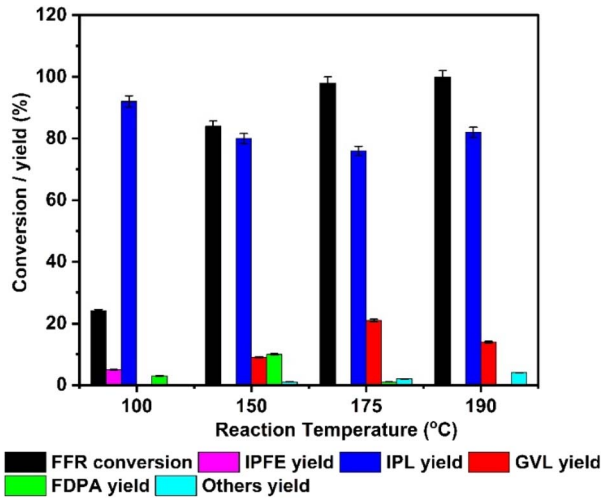

Fig. 3 Effect of reaction temperature on furfural conversion and product yield (reaction conditions: FFR = 100 mg (1 mmol), IPA = 20 mL, catalyst wt. = 100 mg, Time = 6 h).

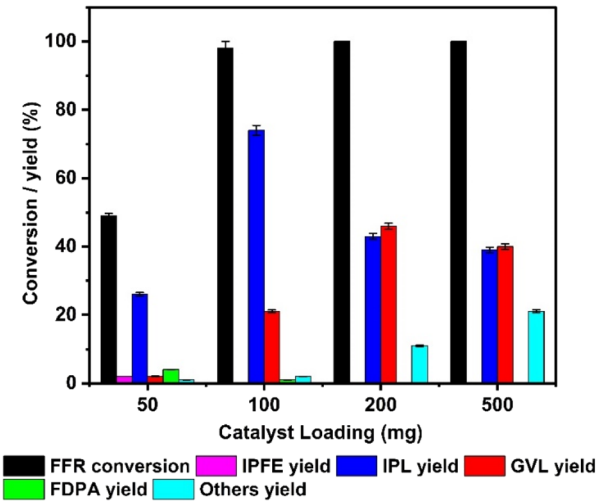

Fig. 4 Effect of catalyst loading on furfural conversion and product yield. (Reaction conditions: FFR = 100 mg (1 mmol), IPA = 20 mL, temp. = 175 °C, time = 6 h).

the yields of FDPA and IPFE are 3 ± 0.06% and 5 ± 0.1% respectively, and their yields decreased while moving to higher temperatures. From the reaction temperature influence study, it can be concluded that IPL can be produced at relatively lower temperature such as 100 °C on TY700 but higher temperature is required to convert IPL to GVL.

The influence of catalyst loading was studied by varying the weight of TY700 from 50 mg to 500 mg while keeping the other reaction parameters same and the results are depicted in Fig. 4. At the lower catalyst loading of 50 mg, the conversion of furfural was only 49 ± 0.1%, with 26 ± 0.5% yield of IPL and 2 ± 0.1% yield of GVL. Increasing the catalyst loading significantly increased the conversion of FFR and it reached 98 ± 2% at 100 mg and 100% at still higher loadings (200 & 500 mg). As a general trend, increasing the catalyst loading increased the yield of GVL. The maximum yield of GVL, 46 ± 0.1% was obtained when catalyst loading was 200 mg. However, at the same time, the yield of unwanted side products (others) started to increase at 200 and 500 mg loadings. The fall in GVL yield at higher catalyst loading may be due to the conversion of GVL to further products. Formation of IPFE (>2%) was observed only at 50 mg catalyst loading. FDPA yield also decreased from 4 ± 0.08% to 1 ± 0.02% when catalyst loading was changed from 50 to 100 mg.

To understand the course of the reaction, the reaction was performed for 12 h under the optimized conditions (FFR = 100 mg (1 mmol), IPA = 20 mL, catalyst wt. = 100 mg, temp. = 175 °C), the conversion of FFR and yields of the products were analysed at regular intervals and the results are plotted in Fig. 5. Initially, after 1 h of reaction, the conversion of FFR was 90 ± 2% and it reached 100% at 8 h reaction time. The yield of IPL and GVL gradually increased while increasing the reaction time from 1 to 6 h. After 6 h, the yield of IPL started to decrease steadily and the same time the GVL yield begun to increase steeply.

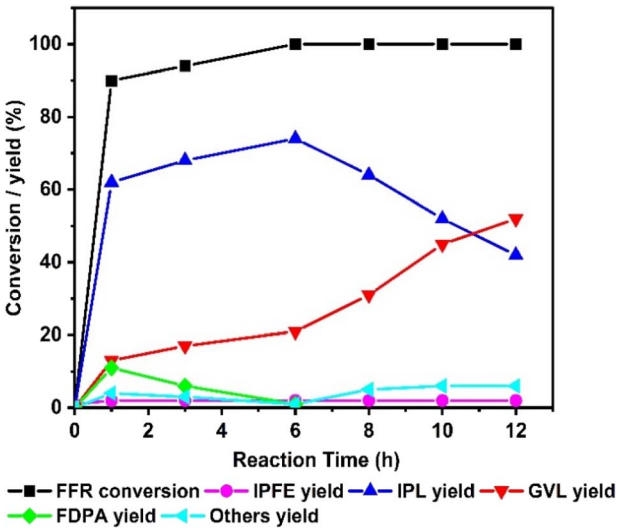

Fig. 5 Effect of reaction time on furfural conversion and product yield (reaction conditions: FFR = 100 mg (1 mmol), IPA = 20 mL, catalyst wt. = 100 mg, temp. = 175 °C).

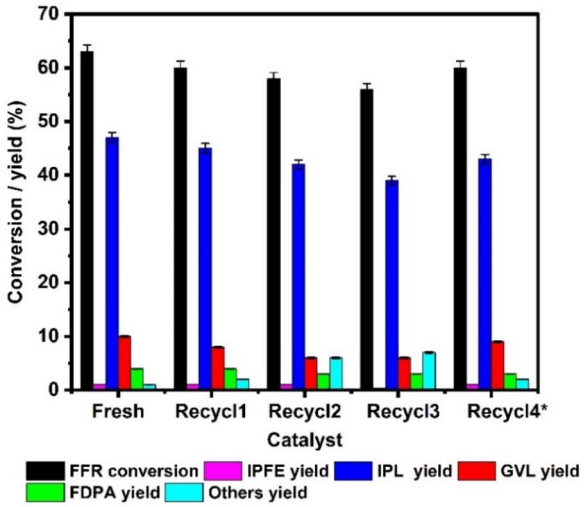

Fig. 6 Reusability of the catalyst in MPV reduction of furfural to γ-valerolactone (reaction conditions: FFR = 100 mg (1 mmol), IPA = 20 mL, catalyst wt. = 65 mg, temp. = 175 °C, time = 6 h).

The yields of IPL and GVL crossover after 10 h and the maximum GVL yield of 52 ± 2% was achieved at 12 h. This observation suggests that IPL is the major product formed initially and it is converted into GVL during the course of the reaction. The yield of FDPA decreased from 11 ± 0.5% to <1% while increasing the reaction time from 1 to 6 h indicating its conversion into the next higher product as shown in Scheme 1. The yield of IPFE was found to be low ~1% thorough out the course of the reaction. It was also observed that the yield of unidentified products (others) is <1% initially and it slightly increases to 2 ± 0.1% after 12 h.

4. Reusability of the catalyst

The reusability of TY700 was investigated and the results are depicted in Fig. 6. The catalyst loading was adjusted to achieve a FFR conversion less than 65%. In the fresh run, TY700 catalyst gave 63 ± 1% FFR conversion and 10 ± 0.2% GVL yield. The catalyst was filtered out of the reaction mixture after the completion of the fresh run, washed with IPA, dried at 100 °C for overnight, and then reused in the following cycle. In this manner, recyclability of the spent catalyst was tested for up to three cycles. The conversion of FFR dropped from 63 ± 1% to 60 ± 1%, 58 ± 1%, 56 ± 1% during the consecutive runs and the yield of GVL dropped from 10 ± 0.2% to 8 ± 0.1%, 6 ± 0.1% and 5 ± 0.1% indicating some loss in catalytic activity. However, when the spent catalyst after three recycles was regenerated by heat treatment in the presence of air at 500 °C (Recycle 4*), it showed an improved conversion FFR (60 ± 1%) and GVL yield (9 ± 0.1%), which is close to that of the fresh catalyst.

5. Comparison with other reported catalysts

Table 4 summarizes the results obtained in this study on TY700 and some of the previous reports on catalytic transfer hydrogenation of furfural over different catalysts, in which Lewis acidic metal ions, $Zr^{4+}$and Sn^{4+}, were used as catalytic active sites. The conversion obtained on TY700 is comparable to other reported catalysts. However, direct comparison of the selectivity of GVL on the different catalysts cannot be fair as it

Table 4 Comparison of the performance of catalysts

Sl. no.	Catalyst	Reaction temp. (°C)	Reaction time (h)	Surface area ($m^2\ g^{-1}$)	Conversion of FFR (%)	Selectivity of GVL (%)	Ref.
1	Zr–Al-beta	170	4	685	100	70	12
2	Zr–Al-beta	170	24	539	100	23	57
3	ZrO_2–SBA-15	130	7	349	93	3	61
4	Zr–SBA-15	190	24	605	99	93	62
5	Au/ZrO_2–ZSM-5	120	24	372	100	78	58
6	HZ-ZrP-16	180	14	251	100	64	63
7	ZrO_2/TPA-beta	170	10	392	100	90	60
8	ZrO_2-[Al]MFI-NS	170	36	510	100	83	27
9	Sn–Al-beta	180	24	486	100	54	23
10	TY700	175	12	713	100	52	Present work

is influenced by different reaction parameters such as, temperature, time, and furfural to catalyst ratio. Even though this limitation is considered, still TY700 catalyst's ease of preparation and recyclability outweigh the other catalysts.

6. Conclusions

Ammonium form of Y, beta and mordenite zeolites were thermally dealuminated in a controlled manner to modify their acid sites. Data obtained from TPD of NH_3 indicated a gradual decrease in total number of acid sites upon increasing the treatment temperature due to dislodgement of aluminium from the tetrahedral framework. There is a drop in the percentage of strong acid sites and at the same time rise in the percentage of weak acid sites while increasing thermal and steam treatment temperature. The treatment temperature does not influence the distribution of moderate acid sites in all three types of zeolites much. ^{27}Al MAS NMR study showed that in Y zeolites, while increasing the thermal treatment temperature from 500 to 700 °C, more framework associated penta-coordinated Al sites and extra-framework octahedral Al sites are generated. TY700 showed the lowest (Al^{IV}-I + Al^{IV}-II)/(Al^{V} + Al^{VI}) ratio (0.96) compared to all the other prepared catalysts, which indicates that it has more Al dislodged from the tetrahedral zeolite framework.

Isopropyl levulinate (IPL) was obtained as the major product whereas furfural diisopropyl acetal, isopropyl furfuryl ether and γ-valerolactone were minor products on all the catalysts studied. No furfuryl alcohol was detected over any of the catalysts under the studied reaction conditions. Hence, cascade reaction starts from acetalization of furfural rather than MPV reduction of furfural to furfuryl alcohol. There is a linear relationship between TOF_{FFR} and weak + moderate acid sites to strong acid sites ratio ((W + M)/S ratio). Overall, weakening the acid sites by dealumination improves the conversion of furfural. However, in TY800, this trend is not followed probably due to its much higher, more than optimum (W + M)/S ratio. Though IPL was the major product formed over all the different framework zeolites studied, GVL was formed only on Y zeolites. In this aspect, TY700 was found to be the most active catalyst. The better catalytic activity of TY700 compared to other catalysts studied could be due to combination different factors such as its framework structure, suitable (W + M)/S acid sites ratio, presence of both Al^{V} and Al^{VI} sites and proper balance between Brønsted and Lewis acid sites. The valorisation of furfural on TY700 catalyst was studied under different reaction conditions to optimize and maximize furfural conversion and GVL yield. 100% furfural conversion and 52% GVL yield was achieved in the following reaction conditions: furfural = 1 mmol, IPA = 20 mL, TY700 catalyst = 100 mg, temperature = 175 °C, time = 12 h. Further, the TY700 catalyst could be recycled for three consecutive runs with small loss in its catalytic activity. Catalytic activity of the spent catalyst could be restored close to that of fresh catalysts, when the spent catalyst after three recycles was regenerated by heat treatment in the presence of air at 500 °C.

Data availability

The data supporting this article have been included as part of the ESI.†

Author contributions

The manuscript was written through contributions of all authors. Malu T. J.: data curation, methodology, investigation, writing – original draft Cheralathan K. K.: conceptualization, resources, supervision, validation, writing – review & editing. All authors have given approval to the final version of the manuscript.

Conflicts of interest

There are no conflicts of interest to declare.

Acknowledgements

The authors thank VIT for providing seed grant (VIT Seed Grant No.: SG20220044) for carrying out this research work. The authors acknowledge Sophisticated Instrumentation Facility (SIF), VIT, Vellore, India, NMR facility in IISC, Bangalore, India, TPD facility in CRF, IIT, Delhi, India, and nitrogen adsorption analysis facility in Material Analysis & Research Centre, Bengaluru, India for their help in characterization. The authors also wish to thank Prof. Masaru Ogura, Institute of Industrial Science, The University of Tokyo, Japan for pyridine-FTIR analysis.

References

1 Z. Fang and X. Qi, *Production of Platform Chemicals from Sustainable Resources*, Springer Singapore, 2017.
2 F. H. Isikgor and C. R. Becer, *Polym. Chem.*, 2015, **6**, 4497–4559.
3 M. J. Climent, A. Corma and S. Iborra, *Green Chem.*, 2014, **16**, 516–547.
4 D. M. Alonso, J. Q. Bond and J. A. Dumesic, *Green Chem.*, 2010, **12**, 1493–1513.
5 G. Dedes, A. Karnaouri and E. Topakas, *Catalysts*, 2020, **10**, 1–25.
6 L. Moghaddam, J. Rencoret, V. R. Maliger, D. W. Rackemann, M. D. Harrison, A. Gutiérrez, J. C. Del Río and W. O. S. Doherty, *ACS Sustain. Chem. Eng.*, 2017, **5**, 4846–4855.
7 W. Yu, K. Xiong, N. Ji, M. D. Porosoff and J. G. Chen, *J. Catal.*, 2014, **317**, 253–262.
8 Y. Nakagawa, K. Takada, M. Tamura and K. Tomishige, *ACS Catal.*, 2014, **4**, 2718–2726.
9 R. F. Perez and M. A. Fraga, *Green Chem.*, 2014, **16**, 3942–3950.
10 X. Li, P. Jia and T. Wang, *ACS Catal.*, 2016, **6**, 7621–7640.
11 J. K. Zeitsch, *The Chemistry and Technology of Furfural and its Many By-Products*, 2000.

12 J. A. Melero, G. Morales, J. Iglesias, M. Paniagua and C. López-Aguado, *Ind. Eng. Chem. Res.*, 2018, **57**, 11592–11599.
13 Y. Nakagawa, M. Tamura and K. Tomishige, *ACS Catal.*, 2013, **3**, 2655–2668.
14 W. Cao, W. Luo, H. Ge, Y. Su, A. Wang and T. Zhang, *Green Chem.*, 2017, **19**, 2201–2211.
15 Z. Lin, X. Cai, Y. Fu, W. Zhu and F. Zhang, *RSC Adv.*, 2017, **7**, 44082–44088.
16 A. O'Driscoll, J. J. Leahy and T. Curtin, *Catal. Today*, 2017, **279**, 194–201.
17 M. J. Gilkey and B. Xu, *ACS Catal.*, 2016, **6**, 1420–1436.
18 J. Song, L. Wu, B. Zhou, H. Zhou, H. Fan, Y. Yang, Q. Meng and B. Han, *Green Chem.*, 2015, **17**, 1626–1632.
19 K. Gupta, R. K. Rai and S. K. Singh, *ChemCatChem*, 2018, **10**, 2326–2349.
20 G. Giorgianni, S. Abate, G. Centi, S. Perathoner, S. Van Beuzekom, S. H. Soo-Tang and J. C. Van Der Waal, *ACS Sustain. Chem. Eng.*, 2018, **6**, 16235–16247.
21 W. Tolek, W. Auppahad, P. Weerachawanasak, O. Mekasuwandumrong, P. Praserthdam and J. Panpranot, *Catalysts*, 2023, **13**(3), 498.
22 S. Song, L. Di, G. Wu, W. Dai, N. Guan and L. Li, *Appl Catal B*, 2017, **205**, 393–403.
23 H. P. Winoto, B. S. Ahn and J. Jae, *J. Ind. Eng. Chem.*, 2016, **40**, 62–71.
24 A. Saotta, A. Allegri, F. Liuzzi, G. Fornasari, N. Dimitratos and S. Albonetti, *ChemEngineering*, 2023, **7**(2), 23.
25 Y. Wang, D. Zhao, D. Rodríguez-Padrón and C. Len, *Catalysts*, 2019, **9**(10), 796.
26 J. Hidalgo-Carrillo, A. Parejas, M. J. Cuesta-Rioboo, A. Marinas and F. J. Urbano, *Catalysts*, 2018, **8**(11), 539.
27 K. D. Kim, J. Kim, W. Y. Teoh, J. C. Kim, J. Huang and R. Ryoo, *RSC Adv.*, 2020, **10**, 35318–35328.
28 R. López-Asensio, J. A. Cecilia, C. P. Jiménez-Gómez, C. García-Sancho, R. Moreno-Tost and P. Maireles-Torres, *Appl. Catal., A*, 2018, **556**, 1–9.
29 M. Koehle and R. F. Lobo, *Catal. Sci. Technol.*, 2016, **6**, 3018–3026.
30 H. Zhang, W. Yang, I. I. Roslan, S. Jaenicke and G. K. Chuah, *J. Catal.*, 2019, **375**, 56–67.
31 A. García, R. Sánchez-Tovar, P. J. Miguel, E. Montejano-Nares, F. Ivars-Barceló, J. A. Cecilia, B. Torres-Olea and B. Solsona, *Fuel*, 2023, **352**, 129045.
32 L. Bui, H. Luo, W. R. Gunther and Y. Román-Leshkov, *Angew. Chem., Int. Ed.*, 2013, **52**, 8022–8025.
33 J. M. Guarinos, F. G. Cirujano, A. Rapeyko and F. X. Llabrés i Xamena, *Mol. Catal.*, 2021, **515**, 111925.
34 M. Popova, I. Trendafilova, M. Oykova, Y. Mitrev, P. Shestakova, M. R. Mihályi and Á. Szegedi, *Molecules*, 2022, **27**(17), 5383.
35 G. Morales, J. A. Melero, J. Iglesias, M. Paniagua and C. López-Aguado, *React. Chem. Eng.*, 2019, **4**, 1834–1843.
36 C. López-Aguado, M. Paniagua, J. A. Melero, J. Iglesias, P. Juárez, M. L. Granados and G. Morales, *Catalysts*, 2020, **10**(6), 678.
37 S. R. Batool, V. L. Sushkevich and J. A. van Bokhoven, *J. Catal.*, 2022, **408**, 24–35.
38 M. T. Jayakumari and C. Kanakkampalayam Krishnan, *Appl. Catal., A*, 2023, **663**, 119318.
39 M. Ravi, V. L. Sushkevich and J. A. van Bokhoven, *Nat. Mater.*, 2020, **19**, 1047–1056.
40 (*a*) C. Deng, J. Zhang, L. Dong, M. Huang, B. Li, G. Jin, J. Gao, F. Zhang, M. Fan, L. Zhang and Y. Gong, *Sci. Rep.*, 2016, **6**(1), 23382; (*b*) D. Liu, P. Yuan, H. Liu, J. Cai, D. Tan and T. Chen, *Appl. Clay Sci.*, 2013, **80**, 407–412; (*c*) O. Ojelabi, S. Yousatit, U. Rashid and C. Ngamcharussrivichai, *Catalysts*, 2023, **13**, 982.
41 (*a*) J. B. Condon, *Surface Area and Porosity Determinations by Physisorption: Measurements and Theory, the Boulevard, Langford Lane*, Kidlington, 2006; (*b*) S. Bhogeswararao and D. Srinivas, *J. Catal.*, 2015, **327**, 65–77.
42 A. Sartbaeva, N. H. Rees, P. P. Edwards, A. J. Ramirez-Cuesta and E. Barney, *J. Mater. Chem. A*, 2013, **1**, 7415–7421.
43 K. Mlekodaj, J. Dedecek, V. Pashkova, E. Tabor, P. Klein, M. Urbanova, R. Karcz, P. Sazama, S. R. Whittleton, H. M. Thomas, A. V. Fishchuk and S. Sklenak, *J. Phys. Chem. C*, 2019, **123**, 7968–7987.
44 P. Cao, L. Lin, H. Qi, R. Chen, Z. Wu, N. Li, T. Zhang and W. Luo, *ACS Catal.*, 2021, **11**, 10246–10256.
45 M. J. Taylor, L. J. Durndell, M. A. Isaacs, C. M. A. Parlett, K. Wilson, A. F. Lee and G. Kyriakou, *Appl. Catal., B*, 2016, **180**, 580–585.
46 R. Kosydar, E. Lalik, J. Gurgul, T. Szumełda and A. Drelinkiewicz, *Int. J. Hydrogen Energy*, 2024, **60**, 293–307.
47 H. Song, F. Jin, Q. Liu and H. Liu, *Mol. Catal.*, 2021, **513**, 111752.
48 J. M. Rubio-Caballero, S. Saravanamurugan, P. Maireles-Torres and A. Riisager, *Catal. Today*, 2014, **234**, 233–236.
49 I. D. Kopa, R. Y. Barakov, S. O. Sotnik and N. D. Shcherban, *Mater. Today Proc.*, 2022, **62**, 7686–7690.
50 M. Ravi, V. L. Sushkevich and J. A. Van Bokhoven, *J. Phys. Chem. C*, 2019, **123**, 15139–15144.
51 Y. Oumi, S. Nemoto, S. Nawata, T. Fukushima, T. Teranishi and T. Sano, Effect of the framework structure on the dealumination-realumination behavior of zeolite, *Mater. Chem. Phys.*, 2002, **78**, 551–557.
52 M. Ravi, V. L. Sushkevich and J. A. van Bokhoven, *Chem. Sci.*, 2021, **12**, 4094–4103.
53 A. V. Yakimov, M. Ravi, R. Verel, V. L. Sushkevich, J. A. Van Bokhoven and C. Copéret, *J. Am. Chem. Soc.*, 2022, **144**, 10377–10385.
54 B. Gil, S. I. Zones, S. J. Hwang, M. Bejblová and J. Čejka, *J. Phys. Chem. C*, 2008, **112**, 2997–3007.
55 Y. Kubota, K. Itabashi, S. Inagaki, Y. Nishita, R. Komatsu, Y. Tsuboi, S. Shinoda and T. Okubo, *Chem. Mater.*, 2014, **26**, 1250–1259.
56 S. R. Batool, V. L. Sushkevich and J. A. van Bokhoven, *ACS Catal.*, 2024, **14**, 678–690.
57 B. Hernández, J. Iglesias, G. Morales, M. Paniagua, C. López-Aguado, J. L. García Fierro, P. Wolf, I. Hermans and J. A. Melero, *Green Chem.*, 2016, **18**, 5777–5781.

58 S. Zhu, Y. Xue, J. Guo, Y. Cen, J. Wang and W. Fan, *ACS Catal.*, 2016, **6**, 2035–2042.
59 X. Li, X. Yuan, G. Xia, J. Liang, C. Liu, Z. Wang and W. Yang, *J. Catal.*, 2020, **392**, 175–185.
60 B. Srinivasa Rao, P. Krishna Kumari, P. Koley, J. Tardio and N. Lingaiah, *Mol. Catal.*, 2019, **466**, 52–59.
61 J. Iglesias, J. A. Melero, G. Morales, M. Paniagua, B. Hernández, A. Osatiashtiani, A. F. Lee and K. Wilson, *Catal. Sci. Technol.*, 2018, **8**, 4485–4493.
62 Z. Liu, Z. Zhang, R. Fu, J. Xu, J. Lu, Z. Wen and B. Xue, *ACS Appl. Nano Mater.*, 2023, **6**, 13196–13207.
63 L. Ye, Y. Han, H. Bai and X. Lu, *ACS Sustain. Chem. Eng.*, 2020, **8**, 7403–7413.